NANO LETTERS

Letter

pubs.acs.org/NanoLett

Entropy-Driven Crystallization Behavior in DNA-Mediated Nanoparticle Assembly

Ryan V. Thaner,[†,§] Youngeun Kim,[‡,§] Ting I. N. G. Li,[‡,§] Robert J. Macfarlane,[†,⊥,§] SonBinh T. Nguyen,[†,§] Monica Olvera de la Cruz,[‡,§] and Chad A. Mirkin*[,†,‡,§]

[†]Department of Chemistry, [‡]Department of Materials Science and Engineering, and [§]The International Institute of Nanotechnology, Northwestern University, 2145 Sheridan Road, Evanston, Illinois 60208-3113, United States

Supporting Information

ABSTRACT: Herein, we report an example of entropy-driven crystallization behavior in DNA-nanoparticle superlattice assembly, marking a divergence from the well-established enthalpic driving force of maximizing nearest-neighbor hybridization connections. Such behavior is manifested in the observation of a non-close-packed, body-centered cubic (bcc) superlattice when using a system with self-complementary DNA linkers that would be predicted to form a close-packed, face-centered cubic (fcc) structure based solely on enthalpic considerations and previous design rules for DNA-linked particle assembly. Notably, this unexpected phase behavior is only observed when employing long DNA linkers with unpaired "flexor" bases positioned along the length of the DNA linker that increase the number of microstates available to the DNA ligands. A range of design conditions are tested showing sudden onsets of this behavior, and these experiments are coupled with coarse-grained molecular dynamics simulations to show that this entropy-driven crystallization behavior is due to the accessibility of additional microstates afforded by using long and flexible linkers.

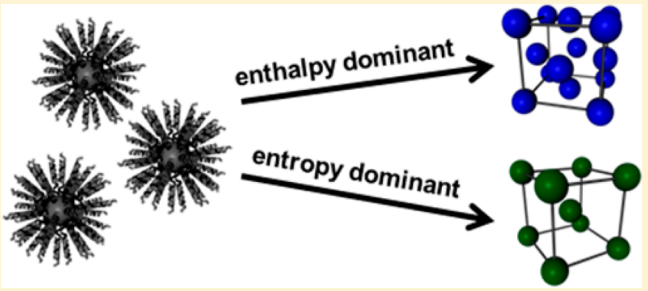

KEYWORDS: *DNA, nanoparticle superlattice, nanomaterials, colloidal crystals, self-assembly*

The field of DNA-mediated nanoparticle crystallization has led to a breadth of superlattice symmetries, both with and without atomic counterparts, giving rise to the term "programmable atom equivalent" (PAE) to describe an individual building block.[1−14] Such constructs are typically composed of a nanoparticle core with synthetic oligonucleotides coating the surface and oriented in the shape of the chosen nanoparticle template.[6] These PAE cores can include nanoparticles of many different compositions, including metals, semiconductors, hollow "spacers", and even proteins, allowing one to deliberately make hundreds of different crystal lattices.[7−9] Unlike molecular and atomic systems, PAEs are a unique platform in which design components of both the core (e.g., nanoparticle shape, size, and composition), and DNA ligands (e.g., nucleobase sequence and surface density) can all be modulated at will, which allows the identity of the building blocks and their bonding behavior to be independently tuned.[10−13] As a result, design rules have been established as to provide predictability along with the ability to synthesize superlattices with independently controllable lattice parameters and crystallographic symmetries.[14,15]

An important feature of the PAE assembly process that has enabled the predictability and exquisite control over superlattice design is that most observed crystal phases operate under the following guiding principle: "The thermodynamic product is one that maximizes the number of nearest neighbor connections."[14] Although many other atomic, molecular, or nanoparticle-based methods for materials assembly involve a complex interplay of several types of forces dictating lattice stability (making predictability challenging), this principle of PAE assembly essentially states that the enthalpy associated with DNA hybridization is the dominant contributor in dictating the thermodynamically preferred state of a given set of PAEs. Thus, predicting lattice stability using solely this parameter has proven to be a reliable guide for superlattice design in the vast majority of cases explored with this system to date.[14,16] For example, in the case of a single-component, self-complementary system, the close-packed, face-centered cubic (fcc) crystal phase is favored, whereas in a two-component, nonself-complementary system consisting of particles of the same size, the non-close-packed, body-centered cubic (bcc) lattice is observed, as each of these structures maximizes DNA hybridization for their respective nanoparticle combinations.[4,14] However, an interesting exercise and challenge to the community is to explore conditions where this guiding principle no longer applies, and other factors beyond maximizing DNA hybridization become significant in dictating lattice stability. We hypothesize that one example should be in systems with long

Received: May 29, 2015
Revised: June 16, 2015

DOI: 10.1021/acs.nanolett.5b02129
Nano Lett. XXXX, XXX, XXX−XXX

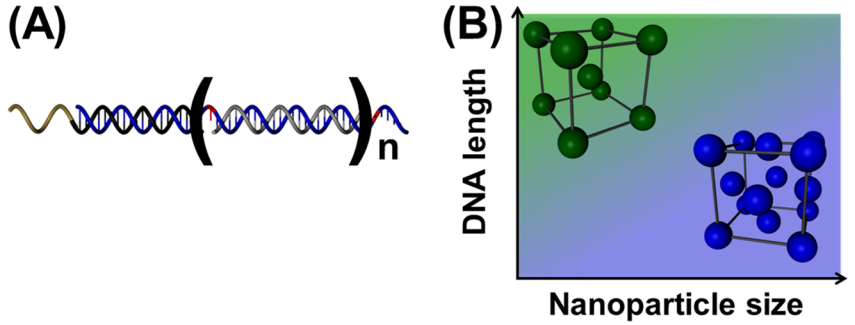

Figure 1. (A) Each linker strand (blue segment) is composed of several regions: an 18-base recognition sequence to hybridize with the particle-bound strand (black and gold segment), a terminal single-stranded "sticky end" to engage in interparticle interactions, and a spacer region to controllably adjust the desired DNA length through the incorporation of 20-base blocks between the recognition region and the sticky end (gray segment), each separated by an unpaired "flexor" base (red segment) to provide flexibility to the linker strand during particle assembly and crystallization. (B) All systems contained self-complementary sticky ends ("GCGC") in this work, which would be predicted to form fcc lattices in order to maximize the number of hybridization events between nanoparticles. However, bcc lattices were formed under conditions where the number of microstates occupied by the DNA linkers increased (i.e., increasing the overall length of the linker or decreasing the particle's radius of curvature).

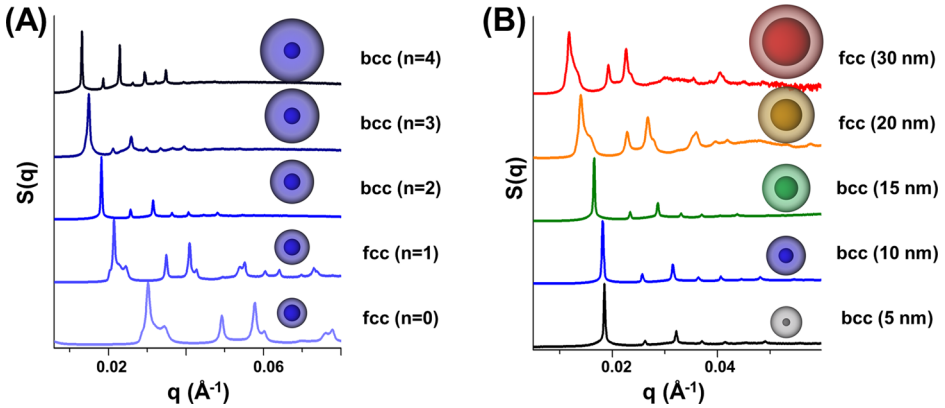

Figure 2. (A) Length of oligonucleotides driving the formation of a nanoparticle superlattice being varied between 6 and 25 nm (n = 0, 1, 2, 3, 4 where n indicates the number of 20-base blocks in the linker strand) while keeping the nanoparticle size constant (10 nm). For short oligonucleotides (n = 0, 1), the sample crystallized into an fcc lattice, whereas longer oligonucleotides (n = 2, 3, 4) formed a bcc lattice. (B) Size of nanoparticles being varied from 5 to 30 nm while keeping the oligonucleotide length constant (n = 2). For nanoparticle sizes of 5, 10, and 15 nm, bcc lattices were formed, whereas 20 and 30 nm particles crystallized into fcc lattices.

and flexible oligonucleotides, where the conformational entropies of the DNA linkers become important.

Herein, we report that the observed crystallization behavior of a specific set of systems with long, flexible DNA linkers cannot be solely explained by the aforementioned guiding principle of maximizing DNA hybridization, and an additional design principle must be considered. In this study, self-complementary systems are observed to yield bcc superlattices as thermodynamic structures despite the ability of a single-component system to form fcc lattices with more nearest neighbors (12 for fcc vs 8 for bcc). In order to investigate the interplay between design parameters and their relative roles in the crystallization process that lead to this unexpected phase formation, a methodical study was carried out by varying DNA length, nanoparticle size, DNA density, and linker rigidity. These experimental results show distinct transition points where the observed thermodynamically preferred phase switches between fcc and bcc as a function of the variables being examined, typically when the length of the DNA linker exceeds that of the inorganic core diameter. Coarse-grained molecular dynamics simulations reveal that enthalpy cannot solely explain the observed bcc phase, and that entropy derived from the additional configurational states of flexible DNA linkers provides subtle but powerful contributions that lead to bcc being favored over fcc even when an fcc lattice would possess greater amounts of DNA hybridization.

Modular iterations to the building blocks and simple correlations to their respective superlattice end states were enabled by the tunability of the PAE platform (Figure 1A). Gold nanoparticles (AuNPs) of different sizes (5−30 nm) were functionalized with the same propylthiol-modified 18-base sequence (Figure 1A; black and gold segment) so that all iterations to the linker were combined with the same nanoparticle stock (full sequences can be found in the Supporting Information). The linker (Figure 1A; blue segment) was composed of a "recognition" region that is complementary to the particle-bound strand on one terminus, and a short "sticky end" which engages in interparticle hybridization events at the other terminus. Situated between these two termini is a spacer region that pushes the sticky end away from the particle surface through the use of "complementary duplexed blocks" (Figure 1A; gray segment) to form rigid duplexes along the length of the linker; this region can be precisely varied to give interparticle spacings with subnanometer control. In this work, a modular spacer region was employed by using 20-base blocks flanked by unpaired "flexor" bases (Figure 1A; red segments)

DOI: 10.1021/acs.nanolett.5b02129
Nano Lett. XXXX, XXX, XXX−XXX

that have been shown to impart a necessary level of flexibility into the system to enable high-quality superlattice formation.[17] Shorthand notation for these systems is used for both clarity and brevity purposes: "*n*" denotes the number of 20-base blocks located between the recognition and sticky end regions. For example, $n = 0$ indicates that only a single flexor base separates these two sections of the linker, whereas $n = 2$ designates that the linker contains two 20-base blocks, each flanked by a flexor base, giving a total of 43 bases in between the recognition and sticky end regions (i.e., 3 flexor bases and two 20-base blocks).

In an initial set of experiments, a screening of systems with variable linker lengths and a constant nanoparticle core size (10 nm) was performed to study the potential effects of each additional 20-base block on the resulting superlattice crystallographic symmetry. Structural analysis of the aggregates with small-angle X-ray scattering (SAXS) showed that in the cases of the shortest linkers ($n = 0$ and $n = 1$), the expected fcc lattice was observed, whereas longer linkers ($n = 2, 3, 4$) surprisingly gave bcc scattering patterns (Figure 2A). Previous work in the field studying the relationship between DNA linker length and nanoparticle core size clearly demonstrated fcc structures for similar systems, but unlike the linker design used in this study, these previous works utilized 40-base complementary blocks to rigidify the linker (see Supporting Information for reproduced results).[15] This distinguishing factor is important and will be discussed later in more detail.

To test that the bcc structure was indeed the thermodynamically favored state and not a kinetically trapped structure, two separate annealing procedures were employed: one process in which the initial disordered aggregate was heated just below its characteristic melting temperature (T_m; as determined by UV–vis melting analysis, see Supporting Information) for approximately an hour and another in which the aggregate was heated above its T_m and allowed to slowly cool through the melting transition over the course of days. The latter approach has recently been shown to form micron-scale single crystals with crystal habits that match their atomic analogue with the same crystal symmetry and therefore provides an experimental means to unequivocally form the thermodynamic structure for a given system.[12] In all systems tested, both annealing procedures gave the same crystal structures, consistent with the assertion that bcc is in fact the thermodynamically favored arrangement for PAEs containing long linkers ($n = 2–4$) on a 10 nm core.

A complementary set of experiments was then designed in which the DNA length ($n = 2$) was held constant but the nanoparticle size was varied. These results showed that fcc structures were formed with 20 and 30 nm particles, whereas bcc lattices were observed for systems containing particles with diameters of 5, 10, and 15 nm. It is important to note that nanoparticles in this size regime have considerably different radii of curvature (e.g., low curvature for bigger particles, high curvature for smaller ones), which has an effect on the volume that individual DNA strands can occupy due to repulsive interactions between neighboring strands.[18] For each DNA length and NP size tested, three different linker loadings were used to investigate the potential effect of linker density on the observed crystal symmetry. Interestingly, only 15 nm AuNPs showed a dependence on the number of linkers added: a bcc structure was observed for the lowest loading, whereas fcc structures were seen for the higher loadings (see Supporting Information for SAXS data).

In addition, the collective understanding gained by probing this wide parameter space informed a final experiment that investigates the role of linker flexibility in a simple but powerful manner. Specifically, the $n = 2$ linker that yielded a bcc structure when added to a 10 nm AuNP, as seen in Figure 2A, was compared with the exact same linker that contained a single 41-base complementary block that fully hybridizes both the two 20-base blocks and the flexor base that normally separates them, thus increasing the overall rigidity of the linker without affecting any other design parameters. As seen previously, the system containing two 20-base blocks yielded a bcc superlattice (Figure 3A); however, the system containing the 41-base block

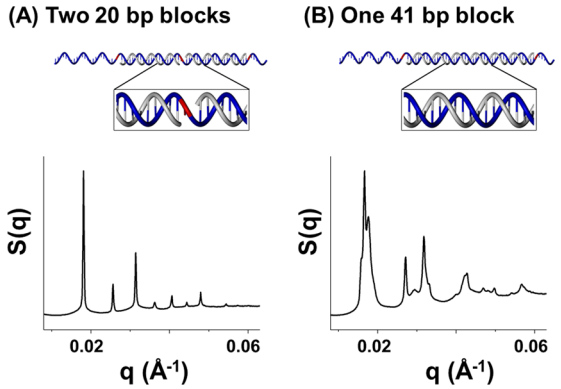

Figure 3. $n = 2$ linker system containing two 20-base blocks (A) was compared with the exact same linker containing a single 41-base block (B) that fully hybridized the two 20-base regions and the flexor base in between them. Note that, with this design, the only difference between the two systems is whether a single flexor base is duplexed or not (and thus the overall rigidity of the DNA strands). The system in (A) yielded a bcc superlattice, whereas the system in (B) formed an fcc lattice.

formed an fcc lattice (Figure 3B, a small amount of the energetically similar hexagonal close-packed (hcp) lattice was also observed).[14] This remarkable result indicates that the difference of only a single base being hybridized or unhybridized on the linker can significantly affect the crystallization behavior such that two different crystal phases can be observed for two nearly identical systems.

Taken together, these experiments outline a general set of conditions that can lead to unexpected bcc lattice formation: long DNA linkers with contour lengths closer to the persistence length of DNA,[19] small nanoparticle cores with higher surface curvature, sparser loading of DNA (in the intermediate AuNP size regime), and a relatively high number of "flexor" bases in the linker. For all of these variables, the transition from fcc to bcc structures correlates with changes that increase the overall flexibility and number of microstates that the DNA linkers can occupy. Although the guiding principle of maximizing DNA hybridization mentioned previously has successfully predicted the preferred lattice structures in most cases reported thus far by considering solely enthalpic contributions to lattice stability, these experimental results suggest that entropy can indeed play an important role in the thermodynamics of crystallization. Though this term is difficult to measure, especially for a complex system with extensive DNA chains,[20,21] one would expect that the contributions from entropy increase as DNA chains become longer and more flexible.[22,23]

In order to gain a better understanding of the role of entropy in these systems, we performed molecular dynamics simulations

DOI: 10.1021/acs.nanolett.5b02129
Nano Lett. XXXX, XXX, XXX–XXX

in which nanoparticles and DNA chains are modeled explicitly. Unlike a mean-field approach, molecular dynamics simulations do not require any assumptions regarding the final result, and consequently, the hypothesis can be tested directly.[24,25] The scale-accurate coarse-grained model we utilized in this study has widely proven itself robust by accurately capturing DNA hybridization kinetics and mapping phase diagrams.[12,16,20,26,27]

To simulate a single-component system, sticky ends were assigned to be self-complementary and matched the sequence used in experiments, "GCGC." The rigidity of the DNA chains, including the duplexed DNA blocks and the single-base "flexors," was carefully tuned using the spring constant parameters in the angle potentials. In order to obtain the nearest-neighbor distance at equilibrium, the first peak position in the pair correlation function was found upon allowing tens of building blocks to relax in a dilute simulation system. Defect-free fcc and bcc superlattices, each with 72 building blocks, were then constructed. Different thermodynamic properties between the two lattices allowed us to probe variations in enthalpy and to infer conformational entropic differences between them. The Nosé−Hoover NVT ensemble at constant temperature with periodic boundary conditions was employed to simulate an equilibrated system. Simulations were performed on HOOMD-blue package on a GPU platform,[28,29] and a typical simulation run took 1 to 2 days.

First, we studied two pairs of systems to mimic and compare several design parameters of the corresponding experiments (details of the molecular model and the simulation system are shown in Figure 4). The first pair included a system containing

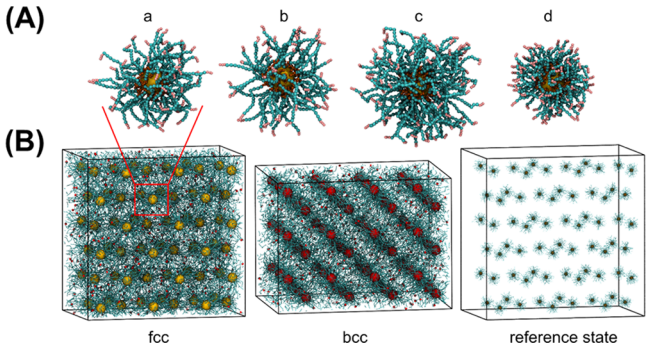

Figure 4. Snapshots of molecular dynamics simulations were generated by rendering with Tachyon ray-tracer. These snapshots show (A) a scale-accurate model of a 10 nm core coated by (a) two 20-base blocks, (b) one 41-base block, (c) three 20-base blocks, and (d) one 20-base block. The detailed designs of the flanking beads on the sticky ends are not shown for clarity. (B) These building blocks were then used to construct the corresponding superlattices and reference states. Interparticle hybridization events are marked in red circles and assembly behaviors were found to be different in the fcc, bcc, and reference state simulations.

two 20-base blocks (20 bp; "a" in Figure 4A) and the other containing a single 41-base block (41 bp; "b" in Figure 4A), with the only difference being a single flexor base being unpaired or paired. This minute difference led to the experimental observation of bcc lattice formation for the former and fcc for the latter. The second pair of systems was simulated using different DNA linker lengths: a system with three 20-base blocks (n = 3, "c" in Figure 4A) and a system with one 20-base block (n = 1, "d" in Figure 4A), which formed bcc and fcc, respectively, in the corresponding experiments. All systems were simulated with both lattices as final states for each linker design (the statistics from the simulations are summarized in Table 1). Although the differences between bcc and fcc systems were subtle, with approximately five independent and identical simulation runs for each system, we were able to obtain results that are statistically significant (i.e., the Welch's t tests[30] gave P-values smaller than 0.0001).

We first note that for all four linker designs listed above, in (a) through (d), fcc had a higher fraction of hybridized DNA linkers (noted as f_H), than the corresponding bcc system, indicating that fcc is always enthalpically favored. As such, the simple guiding principle of maximizing DNA hybridization events properly explains the results for the rigid systems of (b) and (d), which indeed formed fcc structures in experiments. However, experimental results for flexible systems (a) and (c) require an additional explanation because the formation of bcc cannot be explained solely by the guiding principle. Further analysis revealed that the relative enthalpy difference between bcc and fcc lattices (i.e., $\Delta f_H/f_H^{bcc} = (f_H^{fcc} - f_H^{bcc})/f_H^{bcc}$) was smaller in flexible systems (a and c) than in rigid ones (b and d). These smaller differences in f_H suggest that entropic contributions could be more significant in flexible systems and therefore led to the unexpected formation of a bcc lattice as the thermodynamic product.

Due to an enormous number of microstates that can be present in PAE lattices, it is not feasible to directly calculate the entropic difference in such a complex system. Nevertheless, entropic contributions associated with the DNA conformations can be extracted in certain measurable phenomena such as the hydrodynamic radius. Distribution plots of the hydrodynamic radius, R, (i.e., the distance between the end of a DNA chain and the center of the AuNP) for systems, (a) through (d), are shown in Figure 5 (experimental dynamic light scattering (DLS) data for systems (a) and (b) are shown in the Supporting Information). A reference state was constructed by fixing the centers of 72 building blocks far enough away from each other such that each building block is not influenced by its neighbors. In theory, free PAEs in the reference state should possess more entropy than PAEs in ordered fcc or bcc lattices. To make quantitative comparisons related to the conformational entropy of PAEs between the unbound reference state, fcc lattice, and bcc lattice, the conformational entropy was calculated as $S_c = k_B \sum p_i \log(p_i)$, where k_B is the Boltzmann constant and p_i is the probability of a DNA chain being in state i (i.e., the y axis values in Figure 5).[23,31] For all of the four systems tested, S_c^{bcc} was found to be larger than S_c^{fcc}, whereas both lattices had smaller values than S_c^{free} in the reference state. This set of results demonstrated that when considering entropic contributions, bcc is always favored over fcc, contrary to the results regarding enthalpic contributions.

In addition, systems (a) and (c), which formed bcc lattices due to the incorporation of longer and more flexible DNA linkers, had larger conformational entropies than their rigid counterparts. This result validated our assumption that entropy becomes more of a significant factor in flexible systems than in rigid ones, and thus factors beyond the maximization of DNA hybridization need to be considered. This difference was manifested in the distribution curves shifting to larger values (i.e., increased hydrodynamic radii) for bcc systems as compared to those for fcc, which was indeed observed for the flexible systems, (a) and (c), but not found in the rigid systems, as shown in Figure 5. This shift indicates that when a given flexible linker is utilized, an individual building block has a

DOI: 10.1021/acs.nanolett.5b02129
Nano Lett. XXXX, XXX, XXX−XXX

Table 1. Statistical Results From Molecular Dynamics Simulation[a]

system	duplexer	lattice[b]	interparticle distance[c] (nm)	fraction of hybridization f_H	$\Delta f_H / f_H^{bcc}$ [e]	conformational entropy (arbitrary unit)[f]	hydrodynamic volume V (nm^3)	$\Delta V / V^{bcc}$ [g]
a	two20bp	fcc	42.7 (exp.)	0.3695 ± 0.0004	6.30%	18.342 ± 0.006	43,790 ± 15	0.82%
		bcc	42.0 (simu.)	0.3475 ± 0.0004		18.405 ± 0.002	44,150 ± 15	
b	41bp	**fcc**	46.2 (exp.)	0.3467 ± 0.0003	7.90%	17.066 ± 0.005	52,350 ± 15	−0.13%
		bcc	45.2 (simu.)	0.3214 ± 0.0003		17.140 ± 0.005	52,280 ± 10	
c	three20bp	fcc	50.5 (exp.)	0.1890 ± 0.0002	11.80%	19.961 ± 0.004	66,320 ± 25	1.10%
		bcc	48.8 (simu.)	0.1691 ± 0.0002		20.008 ± 0.007	67,050 ± 20	
d	one20bp	**fcc**	33.7 (exp.)	0.3343 ± 0.0001	12.70%	14.206 ± 0.003	25,690 ± 10	−0.27%
		bcc	35.6 (simu.)	0.2966 ± 0.0002		14.338 ± 0.008	25,620 ± 10	

[a]All error bars in the table are standard deviations of approximately five independent and identical simulation runs. [b]Lattice in bold is seen as the thermodynamic symmetry in experiments. [c]First nearest-neighbor distance. Values from experiments are shown on top, values from simulations are shown on the bottom. Coarse grained model has a resolution of bead size ∼2 nm regarding tuning the interparticle distance. [e]$\Delta f_H / f_H^{bcc} = (f_H^{fcc} - f_H^{bcc})/f_H^{bcc}$ [f]Conformational entropy values for the corresponding reference states are 18.905 ± 0.018, 17.413 ± 0.069, 20.209 ± 0.016, 14.528 ± 0.028 for the four systems from top to bottom [g]$\Delta V/V^{bcc} = (V^{bcc} - V^{fcc})/V^{bcc}$

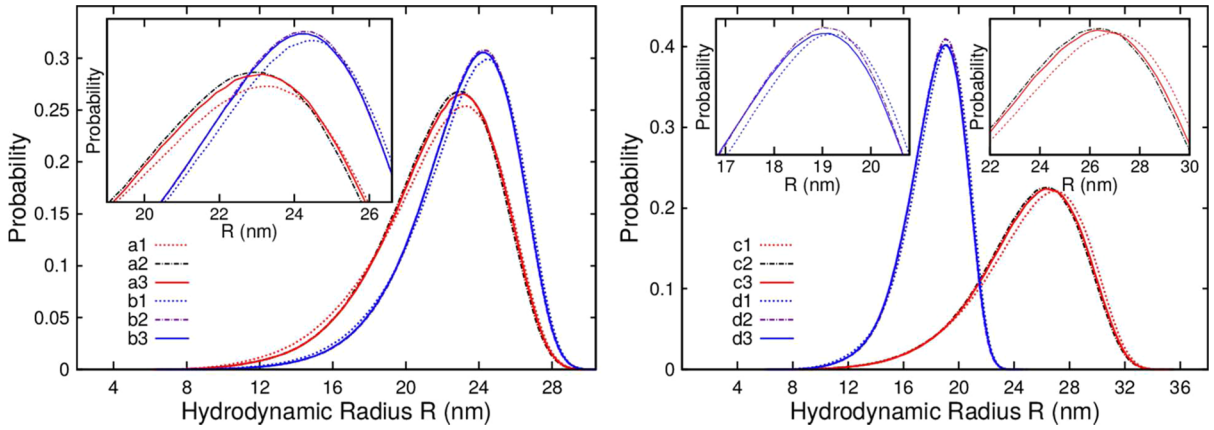

Figure 5. Distribution plots of hydrodynamic radius, R, for a 10 nm AuNP with various DNA designs: systems a and b from Figure 4 (left), as well as systems c and d (right). The plot traces are color-coded and distinguished by line type for each system. The notation, here described for building block "a," is as follows: (a1) represents the reference state of building block, (a2) represents the constructed fcc superlattice, (a3) represents the constructed bcc superlattice. This sequence of terms is paralleled for the other building blocks designs (b), (c), and (d). The peak area of each distribution is zoomed in as shown in the corresponding inset.

larger hydrodynamic volume when arranged in a bcc lattice compared to one in an fcc lattice when the center-to-center distance is kept the same. DNA strands on the building blocks can access more microstates when larger hydrodynamic volumes are occupied, which led to bcc structure formation for systems (a) and (c).

Overall, the experimental results and molecular dynamics simulation data cohesively draw an important lesson regarding the thermodynamics of PAEs. The general thermodynamics equation for the Gibbs free energy of a reaction, $\Delta G = \Delta H - T\Delta S$, consists of both enthalpic (ΔH) and entropic (ΔS) components, which in this case are based on the hybridization events of PAEs during crystallization. Because both of these parameters collectively determine whether a reaction is favorable under a given set of conditions, one can make simple comparisons between ΔG_{fcc} and ΔG_{bcc} to qualitatively determine which final lattice structure is favored to form. For example, in a self-complementary system, the guiding principle of maximizing DNA hybridization events applies when ΔH_{fcc} is notably greater than ΔH_{bcc} ($\Delta H_{fcc} \gg \Delta H_{bcc}$; e.g., 7.9% difference in f_H between fcc and bcc in system (b), as shown in Table 1), which results in the enthalpic term dominating the entropic one and therefore favoring the formation of an fcc lattice (i.e., $\Delta G_{fcc} > \Delta G_{bcc}$). However, when the enthalpic difference between the two lattices is not as significant ($\Delta H_{fcc} > \Delta H_{bcc}$; e.g. 6.3% difference in f_H between fcc and bcc in system (a), as shown in Table 1), the role of the "$-T\Delta S$" term becomes more important than in the previous case. The additional flexibility afforded in the DNA allows the linkers to access more conformational states, resulting in a greater difference between the entropic values (i.e., $\Delta S_{bcc} \gg \Delta S_{fcc}$) and bcc being favored over fcc for these specific systems (i.e., $\Delta G_{bcc} > \Delta G_{fcc}$). Therefore, the subtle difference in the enthalpies of forming fcc over bcc dictates the significance of the entropic contribution to the overall free energy. As the sum of these two energies determines the most thermodynamically stable structure, two different approaches need to be used when explaining crystallization behavior: when the system is enthalpically dominated, design rules and geometric calculations can be applied, but in a system with long, flexible strands, it is crucial to utilize computational models to accurately account for entropic contributions.

It is important to note that an fcc−bcc transition is also seen in the assembly of micelle and star-polymer systems as well as silver nanoparticles capped with alkylthiols of varying length.[32−38] In these polymer systems, researchers reported fcc packing for "crew-cut" micelles and bcc packing for "hairy" micelles.[36] Comparing this to our discussion above for the DNA-coated AuNP system, we find that "soft" shells typically

DOI: 10.1021/acs.nanolett.5b02129
Nano Lett. XXXX, XXX, XXX−XXX

lead to bcc lattice formation, whereas "hard" spheres tend to prefer fcc arrangements.

In conclusion, this study has demonstrated that under specific sets of conditions, contributions beyond the enthalpically centered "maximization of nearest-neighbor interactions" in DNA-directed crystallization of nanoparticles become significant. Specifically, the additional configurational states that are accessed by incorporating long DNA linkers with flexor "pivot points" lead to body-centered cubic superlattice formation in the typically fcc-forming, single-component system. This concept can be illustrated through modular iterations to both the DNA linker length and AuNP size or the strikingly simple difference of a single base being hybridized or not. Molecular dynamics simulations elucidate the underlying subtleties of the thermodynamics of crystallization among these different systems. These results highlight the notion that the region of the linker traditionally considered to be a "passive spacer" for tuning interparticle distances can actually contribute to the energetics of the crystallization pathway. In the current state of the field, while this outlines a region of the vast parameter space that perhaps should be avoided due to the loss of predictability, it also could potentially serve as another tunable design parameter in the programmable assembly of nanomaterials with DNA to determine new structures.

■ ASSOCIATED CONTENT

Supporting Information

Experimental procedures, including oligonucleotide synthesis and purification, nanoparticle functionalization and assembly, small-angle X-ray scattering characterization, and dynamic light scattering measurements are available in the Supporting Information. The Supporting Information is available free of charge on the ACS Publications website at DOI: 10.1021/acs.nanolett.5b02129.

■ AUTHOR INFORMATION

Corresponding Author

*E-mail: chadnano@northwestern.edu.

Present Address

[⊥]Arnold and Mabel Beckman Laboratory of Chemical Synthesis, Division of Chemistry and Chemical Engineering, California Institute of Technology, Pasadena, California 91125, United States.

Author Contributions

R.V.T., Y.K., and T.I.N.G.L. contributed equally.

R.T., Y.K., T.I.N.G.L., R.M., M.O.d.l.C., S.T.N., and C.A.M. designed experiments and wrote the manuscript. S.T.N. coadvised R.T. with C.A.M. R.T. and Y.K. collected experimental data and analyzed data for X-ray studies. T.I.N.G.L. conducted molecular dynamics simulations. All authors have given approval to the final version of the manuscript.

Notes

The authors declare no competing financial interest.

■ ACKNOWLEDGMENTS

This material is based upon work supported by the Air Force Office of Scientific Research Awards FA9550-11-1-0275 and FA9550-12-1-0280; the Department of Defense National Security Science and Engineering Faculty Fellowship award N00014-15-1-0043; and the Center for Bio-Inspired Energy Science (CBES), an Energy Frontier Research Center funded by the U.S. Department of Energy, Office of Science, Basic Energy Sciences award DE-SC0000989-0002. R.V.T. acknowledges a National Science Foundation Graduate Research Fellowship (DGE-1324585). T.I.N.G.L. and Y.K. acknowledge the Ryan Fellowship at the Northwestern University International Institute for Nanotechnology. T.I.N.G.L. acknowledges the Chinese government for the Award for Outstanding Self-Financed Students Abroad.

■ REFERENCES

(1) Macfarlane, R. J.; O'Brien, M. N.; Petrosko, S. H.; Mirkin, C. A. *Angew. Chem., Int. Ed.* **2013**, *52*, 5688.

(2) Mirkin, C. A.; Letsinger, R. L.; Mucic, R. C.; Storhoff, J. J. *Nature* **1996**, *382*, 607.

(3) Tan, S. J.; Campolongo, M. J.; Luo, D.; Cheng, W. *Nat. Nanotechnol.* **2011**, *6*, 268.

(4) Park, S. Y.; Lytton-Jean, A. K. R.; Lee, B.; Weigand, S.; Schatz, G. C.; Mirkin, C. A. *Nature* **2008**, *451*, 553.

(5) Nykypanchuk, D.; Maye, M. M.; van der Lelie, D.; Gang, O. *Nature* **2008**, *451*, 549.

(6) Cutler, J. I.; Auyeung, E.; Mirkin, C. A. *J. Am. Chem. Soc.* **2012**, *134*, 1376.

(7) Brodin, J. D.; Auyeung, E.; Mirkin, C. A. *Proc. Natl. Acad. Sci. U.S.A.* **2015**, *112*, 4564.

(8) Auyeung, E.; Cutler, J. I.; Macfarlane, R. J.; Jones, M. R.; Wu, J.; Liu, G.; Zhang, K.; Osberg, K. D.; Mirkin, C. A. *Nat. Nanotechnol.* **2012**, *7*, 24.

(9) Zhang, C.; Macfarlane, R. J.; Young, K. L.; Choi, C. H. J.; Hao, L.; Auyeung, E.; Liu, G.; Zhou, X.; Mirkin, C. A. *Nat. Mater.* **2013**, *12*, 741.

(10) Macfarlane, R. J.; Thaner, R. V.; Brown, K. A.; Zhang, J.; Lee, B.; Nguyen, S. T.; Mirkin, C. A. *Proc. Natl. Acad. Sci. U.S.A.* **2014**, *111*, 14995.

(11) Kim, Y.; Macfarlane, R. J.; Mirkin, C. A. *J. Am. Chem. Soc.* **2013**, *135*, 10342.

(12) Auyeung, E.; Li, T. I. N. G.; Senesi, A. J.; Schmucker, A. L.; Pals, B. C.; de la Cruz, M. O.; Mirkin, C. A. *Nature* **2014**, *505*, 73.

(13) Auyeung, E.; Macfarlane, R. J.; Choi, C. H. J.; Cutler, J. I.; Mirkin, C. A. *Adv. Mater.* **2012**, *24*, 5181.

(14) Macfarlane, R. J.; Lee, B.; Jones, M. R.; Harris, N.; Schatz, G. C.; Mirkin, C. A. *Science* **2011**, *334*, 204.

(15) Macfarlane, R. J.; Jones, M. R.; Senesi, A. J.; Young, K. L.; Lee, B.; Wu, J.; Mirkin, C. A. *Angew. Chem., Int. Ed.* **2010**, *49*, 4589.

(16) Li, T. I. N. G.; Sknepnek, R.; Macfarlane, R. J.; Mirkin, C. A.; Olvera de la Cruz, M. *Nano Lett.* **2012**, *12*, 2509.

(17) Senesi, A. J.; Eichelsdoerfer, D. J.; Brown, K. A.; Lee, B.; Auyeung, E.; Choi, C. H. J.; Macfarlane, R. J.; Young, K. L.; Mirkin, C. A. *Adv. Mater.* **2014**, *26*, 7235.

(18) Hurst, S. J.; Lytton-Jean, A. K. R.; Mirkin, C. A. *Anal. Chem.* **2006**, *78*, 8313.

(19) Bloomfield, V. A.; Crothers, D. M.; Tinoco, I. *Nucleic Acids: Structures, Properties, and Functions*; University Science Books: Sausalito, CA, 2000.

(20) Li, T. I. N. G.; Sknepnek, R.; Olvera de la Cruz, M. *J. Am. Chem. Soc.* **2013**, *135*, 8535.

(21) Knorowski, C.; Travesset, A. *Soft Matter* **2012**, *8*, 12053.

(22) Ortiz, V.; de Pablo, J. J. *Phys. Rev. Lett.* **2011**, *106*, 238107.

(23) Zhang, J.; Liu, J. S. *PLoS Comput. Biol.* **2006**, *2*, e168.

(24) Shevchenko, E. V.; Talapin, D. V.; Kotov, N. A.; O'Brien, S.; Murray, C. B. *Nature* **2006**, *439*, 55.

(25) Tkachenko, A. V. *Phys. Rev. Lett.* **2011**, *106*, 255501.

(26) Knorowski, C.; Burleigh, S.; Travesset, A. *Phys. Rev. Lett.* **2011**, *106*, 215501.

(27) Knorowski, C.; Travesset, A. *Curr. Opin. Solid State Mater. Sci.* **2011**, *15*, 262.

(28) Anderson, J. A.; Lorenz, C. D.; Travesset, A. *J. Comput. Phys.* **2008**, *227*, 5342.

DOI: 10.1021/acs.nanolett.5b02129
Nano Lett. XXXX, XXX, XXX−XXX

(29) Nguyen, T. D.; Phillips, C. L.; Anderson, J. A.; Glotzer, S. C. *Comput. Phys. Commun.* **2011**, *182*, 2307.
(30) Welch, B. L. *Biometrika* **1947**, *34*, 28.
(31) Suzuki, H. Phase Transition in Gels of Sub-millimeter Size Induced by Interaction with Stimuli. In *Responsive gels: volume transitions II*; Dušek, K.; *Advances in polymer science* 110; Springer: New York, 1993; pp 149−240.
(32) Korgel, B. A.; Fitzmaurice, D. *Phys. Rev. B* **1999**, *59*, 14191.
(33) Bang, J.; Lodge, T. *Macromol. Res.* **2008**, *16*, 51.
(34) Bang, J.; Lodge, T. P. *Phys. Rev. Lett.* **2004**, *93*, 245701.
(35) Bang, J.; Viswanathan, K.; Lodge, T. P.; Park, M. J.; Char, K. *J. Chem. Phys.* **2004**, *121*, 11489.
(36) Lodge, T. P.; Bang, J.; Park, M. J.; Char, K. *Phys. Rev. Lett.* **2004**, *92*, 145501.
(37) Ziherl, P.; Kamien, R. D. *J. Phys. Chem. B* **2001**, *105*, 10147.
(38) Thomas, E. L.; Kinning, D. J.; Alward, D. B.; Henkee, C. S. *Macromolecules* **1987**, *20*, 2934.

DOI: 10.1021/acs.nanolett.5b02129
Nano Lett. XXXX, XXX, XXX−XXX